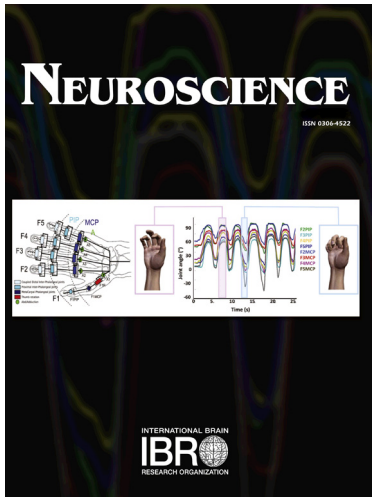

Research Article

Resting-state functional connectivity and deception: exploring individualized deceptive propensity with machine learning

Honghong Tang, Xiaping Lu, Zaixu Cui, Chunliang Feng, Qixiang Lin, Xuegang Cui, Song Su, Chao Liu

PII: S0306-4522(18)30706-1
DOI: https://doi.org/10.1016/j.neuroscience.2018.10.036
Reference: NSC 18713

To appear in: *Neuroscience*

Received Date: 18 September 2018
Accepted Date: 21 October 2018

Please cite this article as: H. Tang, X. Lu, Z. Cui, C. Feng, Q. Lin, X. Cui, S. Su, C. Liu, Resting-state functional connectivity and deception: exploring individualized deceptive propensity with machine learning, *Neuroscience* (2018), doi: https://doi.org/10.1016/j.neuroscience.2018.10.036

Title

Resting-state functional connectivity and deception: exploring individualized deceptive propensity with machine learning

Abbreviated title

Resting-state functional connectivity and individualized deception

Author names and affiliations

Honghong Tang [1,2], Xiaping Lu[2,3], Zaixu Cui [4], Chunliang Feng[2], Qixiang Lin[2,3], Xuegang Cui[1], Song Su[1*], and Chao Liu [1,2,3*]

[1] Business School, Beijing Normal University, Beijing 100875, China
[2] State Key Laboratory of Cognitive Neuroscience and Learning & IDG/McGovern Institute for Brain Research, Beijing Normal University, Beijing, 100875, China
[3] Center for Collaboration and Innovation in Brain and Learning Sciences, Beijing Normal University, Beijing, 100875, China
[4] Department of Psychiatry, Perelman School of Medicine, University of Pennsylvania, Philadelphia, PA, 19104, USA

*Correspondence to:
Song Su
Business School, Beijing Normal University, Beijing 100875, China
E-mail: sus@bnu.edu.cn
Or
Chao Liu
State Key Laboratory of Cognitive Neuroscience and Learning, Beijing Normal University, Beijing, 100875, China
E-mail: liuchao@bnu.edu.cn

Number of pages: 27
Number of figures, tables: 5/2
Number of words for Abstract, Introduction, and Discussion: 239/917/1149
Total number of words: 4264

Abstract

Individuals show a great heterogeneity in determining to be honest or deceptive in daily life. A large number of studies have investigated the neural substrates of deception; however, the brain networks contributed to the individual difference in deception still remain unclear. The current study tried to address this issue by employing a machine-learning approach to predict individuals' deceptive propensity with topological properties of whole-brain resting-state functional connectivity (RSFC). Participants finished the resting-state functional MRI (fMRI) data acquisition, and then played as proposers in a modified ultimatum game in which they spontaneously chose to be honest or deceptive one week later. A linear relevance vector regression (RVR) model was trained and validated to examine the relationship between topological properties of networks of RSFC and actual deceptive behaviors. Results showed that the machine-learning model sufficiently decoded individual differences of deception by using three brain networks based on RSFC, including the executive controlling network (DLPFC, MFC and OFC), the social and mentalizing network (the temporal lobe, TPJ and IPL), and the reward network (putamen and thalamus). These networks have been found to form a signaling cognitive framework of deception by coding mental states of others and the reward or values of deception or honesty, and integrating this information to make final deceptive or honest decisions. These findings suggest the potentiality in using RSFC as a task-independent neural trait to predict deceptive propensity, and shed

light on using machine-learning approaches in deception detection.

Keywords: deception, individual difference, neural trait, machine learning, cross validation, resting-state fMRI

Abbreviations: DLPFC, dorsolateral prefrontal cortex; OFC, orbitofrontal cortex; MFC, middle frontal cortex; IPL, inferior parietal lobule; TPJ, temporo-parietal junction; RSFC, resting-state functional connectivity; ND, nodal degree centrality; NE, nodal efficiency; NB, nodal betweenness centrality; ROIs, regions of interests; LOOCV, leave-one-out cross-validation; RVR, relevance vector regression.

Introduction

People show great individual difference in deception when they have opportunities to lie. Some tell lies all the time while others never lie (Gibson et al., 2013;Greene and Paxton, 2009;Tang et al., 2017). Explicit behavioral cues of individual difference have been widely investigated in deception detection (DePaulo et al., 2003;Newman et al., 2003;Riggio and Friedman, 1983). Progress in cognitive neuroscience techniques in the past decade leads to considerable interest in examining the underlying neural correlates of deception and deception detection (Abe, 2011;Jenkins et al., 2016;Kozel et al., 2005;Langleben, 2008;Ofen et al., 2017;Sun et al., 2015).

By comparing difference of neural responses between lying and telling the truth, most empirical studies indicate that deception recruits multiple brain networks. That is, the prefrontal cortex (e.g., superior frontal cortex (SFC), orbitofrontal cortex (OFC), and middle frontal cortex (MFC)), the anterior cingulate cortex (ACC), the subcortical (e.g., striatum, thalamus, etc.) and posterior cortical regions (e.g., premotor and motor cortex, precuneus, inferior parietal lobule (IPL)), the temporal lobe and temporo-parietal junction (TPJ) (Lisofsky et al., 2014;Spence et al., 2004). These networks are considered to interact with each other to shape deception as an integral system. The prefrontal cortex and ACC are engaged in the executive controlling and behavior inhibiting processes in deception (Christ et al., 2009); the subcortical regions are engaged in processing the reward or benefits of deception (Abe and Greene, 2014); the regions in the temporal and parietal lobe are involved in

dealing with social context and mentalizing intentions and mental states of others (Molenberghs et al., 2016).

Researchers also tried to predict individualized deception with these brain networks. Task-dependent neuroimaging studies show that activities of dorsolateral prefrontal cortex (DLPFC), MFC, parietal lobe and subcortical regions are correlated with the frequency of deception (Abe and Greene, 2014;Cui et al., 2018;Dogan et al., 2016;Greene and Paxton, 2009). However, these studies used different paradigms and experimental designs, making it hard to obtain the general neural networks contributed to deception propensity of each individual. Moreover, several studies using structural brain measures found that neocortex size and white matter volumes in the brain could predict individual deceptive propensity (Byrne and Corp, 2004;Yang et al., 2007), suggesting the possibility to use task-independent neural measures to capture individual difference in deception.

The current study aims to decode the heterogeneity in deception from intrinsic whole-brain functional connectivity. We used topological properties of resting-state functional connectivity (RSFC) calculated by graph theory analysis to predict heterogeneity in deceptive behaviors across individuals (i.e., to differentiate individuals with high and low propensity of deception) with a machine-learning approach.

RSFC is used to characterize the patterns of connections between brain regions in a task-independent state (Biswal et al., 1995), which has been proposed to be an effective neural trait measure to predict individual difference in behaviors (Gabrieli

et al., 2015;Nash et al., 2015). First, RSFC, especially the whole-brain RSFC, is stable and reliable, which has high test-retest reliability (Cao et al., 2014;Zuo and Xing, 2014). Second, it could depict the uniqueness of each individual's brain functional organization, severing as a "fingerprint" in identifying individuals (Finn et al., 2015). Furthermore, it is sufficient to predict mental states and social behaviors such as subjective happiness (Luo et al., 2015), impulsivity in economic decision-making (Li et al., 2013), trust behavior (Hahn et al., 2014), reciprocity of a gift (Cáceda et al., 2015), preference to social information (Zhang and Mo, 2016), and costly punishment for unfair behaviors (Feng et al., 2018). Therefore, we hypothesized that individual difference in deception would be predicted by RSFC patterns between brain networks.

To capture the topological properties of brain networks derived from RSFC, we employed a graph theory analysis and put these properties as features in the prediction of deceptive behaviors. As a framework that depicts organization principles of complex networks, the graph theory could provide a quantitative description of brain with graphs composed of nodes (i.e., regions or voxels) and edges (i.e., functional connectivity between nodes) in several networks (Bullmore and Sporns, 2009;He and Evans, 2010). Three network metrics are commonly used to quantify the topological properties of each network node. That is, the nodal degree centrality (ND) which measures the involvement of a node in the network (Boccaletti et al., 2006;He and Evans, 2010); the nodal efficiency (NE) that estimates the efficiency of parallel information processing of a node in the network

(Achard and Bullmore, 2007); and the nodal betweenness centrality (NB) that assesses the degree of influence a node has on spreading information through the network (Freeman, 1978). These metrics of resting-state brain network has been consistently found to be associated with behaviors (Cao, et al., 2014;Feng, et al., 2018;Liu et al., 2017).

With these network metrics, the current study aims to distinguish individuals with different propensity of deception by a machine-learning approach. The machine-learning approach selects metrics of nodes, then trains predictive models of brain-behavior relationships with training samples and assesses the performance of the model with independent-testing samples through cross-validation (Cui and Gong, 2018;Cui et al., 2018;Cui et al., 2016;Shen et al., 2017). Through these procedures, we hope to obtain the discriminative features in the resting-state brain networks as the neuroimaging makers for deceptive behaviors. Specifically, we hypothesized that metrics of brain networks found in previous deception related studies, i.e., the executive controlling and behavior inhibiting network (e.g., DLPFC, MFC, OFC), the social context and mentalizing network (e.g., the temporal lobe, IPL, TPJ), and the reward network (e.g., putamen, thalamus) would be primarily contributive in the prediction.

Experimental Procedures

Participants

Fifty-two healthy participants from Beijing Normal University (23 females; M_{age} = 23.3, SD = 2.15). Two participants misunderstood the task; three participants

reported that they did not know they could lie in the task. Their data were not included in the analysis. All participants reported no history of neurological or psychiatric disorders, signed consents and were paid with money. The Institutional Review Board of the State Key Laboratory of Cognitive Neuroscience and Learning of Beijing Normal University approved this study.

Procedure

Firstly, all participants were required to keep still and close their eyes to finish a resting-state fMRI scanning session, which lasted for 6 minutes and 46 seconds. They were instructed to not to think about anything systematically or fall asleep during scanning. One week after that, they finished a behavioral test session, during which they played as the proposer in a modified ultimatum game (Güth et al., 1982;Tang et al., 2016;Tang, et al., 2017). They were instructed to divide a total of money units (randomly chosen from 8, 10, 12, or 14 units in each trial) between themselves and anonymous recipients in 12 trials (Figure 1A). The range of the money units would not be shown to them. At the beginning of each trial, they would randomly gain a total amount of money units (True total) from the computer for the division. Then, they needed to report the amount of the total (Reported total) to the recipient who did not know the total amount, which provided a chance for them to tell a lie. Next, they made a division and then waited for the recipient to accept or reject it. If the recipient accepts the division, participants and the recipient would gain the money units according to the division; if the recipient reject it, all of them gained nothing. In each trial, participants' divisions were paired with choices from

52 real recipients collected previously in another study with the same experimental paradigm and were told that recipients would never know the true total they gained. We aimed to measure participants' spontaneous tendency of deception, thus we controlled the rejection rate for each participant with 25% based on real recipients' responses in the previous study. We run at least two participants at the same time to make they believe that they play with real recipients. Each participant sat in a small room to finish the task alone. All participants were debriefed after the whole task. They answered questions including whether they knew they could spontaneously choose to deceive the recipient in the task, whether recipients would know their true totals, and whether recipients' choices would affect their payments.

Image acquisition

The resting-state fMRI scanning was finished at Beijing Normal University Imaging Center for Brain Research with a Siemens Trio 3 T MRI scanner (Lin et al., 2015;Liu, et al., 2017). Firstly, we obtained participants' 3D structural images with 144 sagittal slices by a T1-weighted MP-RAGE sequence. The thickness was 1.33 mm; the in-plane resolution was 256 × 256; the repeat time (TR) was 2530 ms; the echo time (TE) was 3.39 ms; the inversion time (TI) was 1100 ms; the flip angle was 7°; and the FOV was 256 × 256 mm. Next, we sued an echo-planar imaging (EPI) sequence to obtain resting-state MRI data. The axial slices was 33; the thickness was 3.5 mm; the gap was 0.7 mm; the in-plane resolution was 64×64; the voxel size was 3.1 × 3.1 × 3.5 mm; the repeat time (TR) was 2000 ms; the echo time (TE) was 30 ms; the flip angle was 90°; the field of view (FOV) was 200 × 200 mm, and the

volumes was 200.

Behavioral data analysis

We calculated the mean deception degree (Deception degree = (True total - Reported total)/True total) as the index of participants' deceptive tendency. Thus, the higher the deception degree is, the more deceptive the participant.

Imaging data preprocessing

SPM 12 (www.fil.ion.ucl.ac.uk/spm) and DPABI software packages (http://rfmri.org/dpabi) (Yan et al., 2016) were used to preprocess fMRI data. Firstly, we removed the first 10 volumes of the functional images to make signals stable, then corrected images with slice timing and realigned them with head motion correction. Next, we co-registered the mean functional image and segmented structure brain image of each participant. After that, we normalized their functional images onto the Montreal Neurological Institute space and resampled images with a voxel size of 3 x 3 x 3 mm. Then the linear trend of the time courses was removed and a band-pass filter (0.01-0.1 Hz) was used to remove low- or high- frequency noise and artifacts (Biswal, et al., 1995;Zuo et al., 2010). A 4 mm FWHM Gaussian kernel was used to smooth images and reduce spatial noises. Finally, the 24 head motion parameters (Fox et al., 2005), the white matter signal, and the cerebrospinal fluid signal (Friston et al., 1996) were regressed out. Since global signal regression might cause ambiguous negative connections, it was not implemented in the preprocessing (Buckner et al., 2009;Xie et al., 2017).

Network construction

A graph theoretical analysis was used to obtain the brain network based on resting-state functional connectivity , which depicts the brain as graphs that consisting of nodes (brain regions or voxels) and edges (functional connectivity between nodes) (Bullmore and Sporns, 2009;He and Evans, 2010;Wang et al., 2015;Wang et al., 2010). The GRaph thEoreTical Network Analysis toolbox (GRETNA: http://www.nitrc.org/projects/gretna/) was used to construct and analysis brain networks. Firstly, we used a functional brain atlas with 264 non-overlapping regions of interests (ROIs) to define the whole brain network nodes (Power et al., 2011). This atlas was available in the GRETNA, in which each ROI's radius is 3 mm. The BOLD signal for all the voxels in each ROI at each time point was averaged as the time course of each node for each participant. To compute the network edges, the Pearson correlation *r* between ROIs' time courses in the atlas was calculated, resulting into a 264×264 functional connectivity map. After transforming the correlation *r* into Fisher *z* value, functional brain networks indexed by functional connectivity were binarized to run the network analysis. Positive and negative functional connectivity were analyzed separately in both network construction and network analysis.

Network analysis

To characterize the importance of each node in the brain network, three widely used nodal metrics (Nodal degree centrality (ND), Nodal efficiency (NE), Nodal betweenness centrality (NB)) (Figure 2) were calculated based on the binary functional connectivity between nodes in the network (Boccaletti, et al., 2006;He and Evans, 2010). The ND metric refers to the number of edges (connections of a node

connected to other nodes) (Freeman, 1978). The NE metric is the mean of inversed minimum path length between a given node and all other nodes in the network (Achard and Bullmore, 2007). The NB metric is the percentage of all shortest paths of connections that pass through a node (Freeman, 1978). These nodal metrics were used features to predict deception degree in the machine-learning approach as follows.

Relevance vector regression (RVR)

Nodal features ND, NE, NB in the brain network were put into a linear relevance vector regression (RVR) algorithm, which was implemented by the function of PRoNTo toolbox (http://www.mlnl.cs.ucl.ac.uk/pronto/) (Schrouff et al., 2013). RVR is a sparse kernel machine-learning algorithm that has been used to predict behavioral measures with resting-state brain data (Gong et al., 2013). Based on a fully probabilistic Bayesian framework (Tipping, 2001), RVR introduces a mean-zero Gaussian prior over the model weights and each weight corresponds to one training sample. These weights are governed by a set of hyperparameters (one for each model weight) (Tipping, 2001), which are estimated iteratively on the training data. Since the posterior distributions of many of the model weights are sharply peaked around zero, those training samples related with non-zero weights are treated as "relevance vectors". Then, the regression coefficients of all features are determined as the weighted sum of the feature vector of all "relevance vector" samples. For an unseen testing sample, the predicted behavioral score (e.g., predicted deception degree) was defined as the product of these regression coefficients and the feature vector of this sample. Compared to another widely used machine-learning algorithm, the linear

support vector regression (LSVR), RVR has no free parameter and has comparable predictive power and lower computational cost in behavioral predictions with brain functional connectivity (Cui and Gong, 2018).

In the current study, we put ND, NE, NB features into the RVR both separately and together to find the best predictor of behavioral deception degree. We adopted the leave-one-out cross-validation (LOOCV) to evaluate the generalizability of the model. That is, *N*-1 (*N* equals the sample size of participants) participants' data was used as the training data, and the left one was treated as the testing set. Each feature was linearly scaled to the range of 0-1 across the training dataset, and the same scaling parameters were applied to scale the testing set (Cui and Gong, 2018;Cui, et al., 2018). A prediction model was constructed using all the training samples, and was used to predict the scores of the testing sample. The training and testing procedures were repeated *N* times so that each subject was used once as the testing sample. The Pearson correlation coefficient (*r*) and mean absolute error (MAE) between actual and predicted deception degree across all subjects were computed to quantity the accuracy of the prediction (Cui and Gong, 2018;Cui, et al., 2018).

Then a permutation test was used to determine whether the obtained final accuracy metrics (i.e., coefficient *r* and MAE) were significantly better than expected by chance. Specifically, the above prediction procedure was re-applied 1,000 times. For each time, we permuted the behavioral scores across the training samples without replacement. The *P* value for the prediction performance (for both the correlation *r* and MAE) was calculated by dividing the number of times the permuted value was

greater than (or less than, or equal to) the true value by 1000.

For visualization, we colored all ROIs whose model weight in the prediction was higher than 40% of the maximum predicted weight. This threshold predominantly eliminates noise components whose predicted weight was lower than 40% and could visualize the most predictive brain regions (Ecker et al., 2010;Mourão-Miranda et al., 2005).

Validation

To validate our prediction results, a 10-fold cross-validation was applied (Cui, et al., 2018;Feng, et al., 2018). Similar to the LOOCV, this procedure divided all participants into 10 subsets, and used nine of the subsets as the training data and the remaining one as the testing data. It repeated 10 times to let each subset could be used as the testing data once. To avoid the data division affected the prediction performance, we repeated the 10-fold cross-validation for 50 times and used the average results as the final prediction performance. Finally, the significance of the prediction performance was assessed by a 1000 times permutation test.

Results

Behavioral results

The mean deception degree was 0.15 (*SD* = 0.13). The distribution of deception degree showed that 19.1% participants (*n* = 9) never deceived, and 4.2% participants misreported their gained totals as less than 60% of the true totals, indicating great individual difference in deceptive propensity (Figure 1B). No gender (t_{45} = 0.40, *p* = 0.70) or age (*r* = -0.13, *p* = 0.40) difference was found in the deception degree.

Prediction results of RVR

Results of prediction with nodal features derived from positive functional connectivity were shown in Figure 3. The predicted deception degree was highly correlated with the actual behavioral deception degree for ND (r = 0.38, p = 0.009) and NE (r = 0.48, p < 0.001) features, but not for NB features (r = -0.05, p = 0.76). Specifically, combination of ND, NE features also led to significant correlation between predicted and actual deception degree (r = 0.42, p = 0.003), yet combination of ND, NE, and NB features did not (r = 0.29, p = 0.051). Therefore, we focused on reporting the results of the prediction of ND and NE respectively. The permutation test showed that the correlations for ND (Figure 3D) and NE (Figure 3E) were significantly higher than the chance level (permutation tests, p_{ND} = 0.021, p_{NE} = 0.003). No significant correlations between predicted and actual deception degree was found for nodal features derived from negative functional connectivity (rs < 0.26, ps > 0.08).

Predictive nodal features

There were 33 ND features contributed to the RVR prediction (Figure 4A and Table 1), which were derived from the temporal lobe (i.e., bilateral inferior and middle temporal gyrus (MTG), fusiform), subcortical regions (i.e., left putamen and thalamus), frontal lobe (i.e., bilateral precentral gyrus, right OFC, bilateral superior and medial frontal gyrus (including DLPFC, MFC)), parietal lobe (i.e., left precuneus, IPL, TPJ), the occipital lobe and cerebellum. Similar to ND features, 25 NE features contributed to the RVR prediction (Figure 4B and Table 2), which were also originated from the bilateral temporal lobe and right fusiform, left putamen, bilateral

thalamus, right OFC, bilateral superior and medial frontal gyrus, left precuneus, bilateral parietal lobe, occipital gyrus and cerebellum.

Validation

Results of the 10-fold cross-validation showed that the predicted deception degree remained significantly correlated with the actual deception degree for ND (mean $r = 0.33$, permutation test, $p = 0.031$, Figure 5A) and NE (mean $r = 0.43$, permutation test, $p = 0.007$, Figure 5B).

Discussion

Great individual difference has been found in deceptive behaviors, but the neural correlates of it remains unclear. The current study employed a machine-learning approach to predict deceptive propensity at individual level by intrinsic brain network in resting state. We found that graph-theoretical topological properties derived from resting-state brain network were able to predict individual deceptive tendency in an independent experiment. Specifically, individual difference in deception were primarily differentiated by nodal (regional) features across several brain networks, including the executive controlling network (e.g., prefrontal cortex), the social and mentalizing network (e.g. temporal lobe, TPJ, IPL), and the reward network (e.g., putamen, thalamus). These findings suggest that deception recruits interactions between multiple brain networks.

Previous task-dependent deception studies consistently found these brain networks engaged in deception (Baumgartner et al., 2009;Bhatt et al., 2010;Greene and Paxton, 2009;Kozel, et al., 2005;Ofen, et al., 2017;Sun, et al., 2015). The

prefrontal cortex (including the DLPFC, MFC and OFC) is usually regarded as the key network for general deception. It is involved in the executive control processes, including memorizing the truth when generating a lie, suppressing a truthful response, and switching behavioral responses between honesty and deception (Christ, et al., 2009;Greene and Paxton, 2009;Spence, et al., 2004). Specifically, stimulating or damaging the DLPFC could increase or decrease deception (Maréchal et al., 2017;Zhu et al., 2014), indicating its critical role in deciding to be deceptive or honest. As a contrast, the temporal lobe, TPJ and IPL are found to be more specific to interactive deception. They are recruited in socio-cognitive processes in deception, such as reasoning others' intentions, beliefs and goals in social interaction (Bhatt, et al., 2010;Lisofsky, et al., 2014;Molenberghs, et al., 2016;Tang, et al., 2016;Tang, et al., 2017). A recent study also find these regions were engaged in consolidating social information in the resting state (Meyer et al., 2018), reflecting their functions in representing abstract social information for behaviors.

However, few studies paid attentions to the function of subcortical regions such as striatum and thalamus in deception. Some studies found negative relationship between dopamine D2-receptor availability in striatum and the "Lie" scale scores of social responsibility, which measures individuals' tendency to overly behave in a socially desirable way (Cervenka et al., 2010;Egerton et al., 2010;Huang et al., 2006;Reeves et al., 2007). They suggest the function of striatum in differentiating individuals with personality traits related to deception. Recently, neural response of anticipated reward in the dorsal striatum was found to be correlated with response of

dishonest benefits in the DLPFC (Abe, 2011;Abe and Greene, 2014), providing direct evidence for the role of subcortical regions in processing reward seeking for deceptive behaviors.

Consistent with these studies, our results provided the first evidence for the role of these three brain networks in deception with topological properties originated from intrinsic resting-state functional connectivity. These networks interact with each other and then might shape deception in a signaling cognitive framework (Jenkins, et al., 2016) . Firstly, the social and mentalizing network represents the characteristics and mental state of both receivers and themselves, the potential actions and potential results related to deception in the deceivers' mind. Then the reward network decodes the reward or values of different potential actions (e.g., to be honest or deceptive) and forms motivations for each actions. Finally, the two networks send the social and motivational information to the central executive system, which makes the final decision to be deceptive or honest then generate the final behavior (Abe, 2011;Abe and Greene, 2014;Lisofsky, et al., 2014;Spence, et al., 2004). Furthermore, these networks are also active in task-dependent deception studies, implying that neural networks in shaping personality traits related to deceptive propensity in task-independent state may be overlapped rather than being dissociated with networks engaged in making actual decisions to be deceptive or honest (Abe, 2011;Cervenka, et al., 2010;Egerton, et al., 2010;Huang, et al., 2006;Reeves, et al., 2007).

Interestingly, we did not find any topological properties of the anterior cingulate cortex (ACC) in prediction of deceptive propensity. Although both prefrontal cortex

and ACC are greatly active in monitoring cognitive conflict and inhibiting response in deception, their functions are different. The prefrontal cortex is a more general network for different types of deception, whereas the ACC is more specific to deception that requires participants to monitor cognitive conflict to pretend not to know the truth (Abe et al., 2005), or deception that associated with emotional response (Baumgartner, et al., 2009;Kozel, et al., 2005). Therefore, ACC in the task-independent state might not be contributive to deceptive propensity.

In addition, results in the current study demonstrate that RSFC could be used to represent individual difference in social preference and behaviors, which are in line with studies that use RSFC to predict impulsivity (Li, et al., 2013), trust behavior (Hahn, et al., 2014), reciprocity (Cáceda, et al., 2015), and costly punishment (Feng, et al., 2018). These findings suggest the potentiality in using RSFC as a task-independent neural trait to predict deceptive propensity as neocortex size and white matter volumes in the brain (Byrne and Corp, 2004;Nash, et al., 2015;Yang, et al., 2007). Specifically, we employed a machine-learning approach to perform the prediction of brain-behavior relationship at the individual level, which is advantageous in generalizing results into independent new data (Cui and Gong, 2018;Shen, et al., 2017). The usage of this approach not only support the potentiality of predicting social preference and behavior with brain neuroimaging data (Cui, et al., 2018;Feng, et al., 2018), but also shed light on the application of neuroimaging markers in deception detection (Langleben, 2008).

Several limitations should be considered when generalizing and extending results

in this study. First, the behavioral deception degree in the current study captures the deceptive propensity in interactive context, future studies are needed to examine the neural networks underlying both interactive and non-interactive context (Lisofsky, et al., 2014). Second, our results only demonstrate the neural networks associated with actual deception. Future studies combine neural networks contributive to both actual deception and personality traits related to deception would provide more information about how to use neural trait to predict deceptive propensity (Cervenka, et al., 2010;Egerton, et al., 2010;Huang, et al., 2006;Nash, et al., 2015;Reeves, et al., 2007). Thirdly, future studies that focus on the temporal and directional relationship among these networks would demonstrate how they interact with each other in making decisions about deception. Finally, future studies are encouraged to combine the topological properties and other properties of neural networks, and other neuroimaging measures, such as T1-weighted and diffusion-weighted brain data, to achieve a better and reliable network associated with deceptive propensity.

Taken together, this current study indicate that brain networks based on intrinsic resting-state functional connectivity are sufficient to predict individual difference in deceptive propensity. It sheds light on using the machine-learning approach in deception detection and identifying neural trait associated with social preference and behaviors.

Acknowledgments

This work was supported by the National Key R&D Program of China (2017YFC0803402), the National Natural Science Foundation of China (NSFC) (31871094, 31800958, 71572018, 71872016, 71772015), the China Postdoctoral

Science Foundation (2018M630103), the Beijing Municipal Science & Technology Commission (Z151100003915122), the National Program for Support of Top-notch Young Professionals.

Reference

Abe N (2011), How the brain shapes deception: An integrated review of the literature. Neuroscientist 17:560-574. doi:10.1177/1073858410393359

Abe N, Greene JD (2014), Response to anticipated reward in the nucleus accumbens predicts behavior in an independent test of honesty. J Neurosci 34:10564-10572. doi:10.1523/jneurosci.0217-14.2014

Abe N, Suzuki M, Tsukiura T, Mori E, Yamaguchi K, Itoh M, Fujii T (2005), Dissociable roles of prefrontal and anterior cingulate cortices in deception. Cereb Cortex 16:192-199. doi:10.1093/cercor/bhi097

Achard S, Bullmore E (2007), Efficiency and cost of economical brain functional networks. PLoS Comput Biol 3:e17. doi:10.1371/journal.pcbi.0030017

Baumgartner T, Fischbacher U, Feierabend A, Lutz K, Fehr E (2009), The neural circuitry of a broken promise. Neuron 64:756-770. doi:10.1016/j.neuron.2009.11.017

Bhatt MA, Lohrenz T, Camerer CF, Montague PR (2010), Neural signatures of strategic types in a two-person bargaining game. Proc Natl Acad Sci U S A 107:19720-19725. doi:10.1073/pnas.1009625107

Biswal B, Zerrin Yetkin F, Haughton VM, Hyde JS (1995), Functional connectivity in the motor cortex of resting human brain using echo-planar mri. Magn Reson Med 34:537-541. doi:doi:10.1002/mrm.1910340409

Boccaletti S, Latora V, Moreno Y, Chavez M, Hwang DU (2006), Complex networks: Structure and dynamics. Phys Rep 424:175-308. doi:10.1016/j.physrep.2005.10.009

Buckner RL, Sepulcre J, Talukdar T, Krienen FM, Liu H, Hedden T, Andrews-Hanna JR, Sperling RA, et al. (2009), Cortical hubs revealed by intrinsic functional connectivity: Mapping, assessment of stability, and relation to alzheimer's disease. J Neurosci 29:1860-1873. doi:10.1523/jneurosci.5062-08.2009

Bullmore E, Sporns O (2009), Complex brain networks: Graph theoretical analysis of structural and functional systems. Nat Rev Neurosci 10:186. doi:10.1038/nrn2575

Byrne RW, Corp N (2004), Neocortex size predicts deception rate in primates. Proc R Soc Lond B Biol Sci 271:1693-1699. doi:10.1098/rspb.2004.2780

Cáceda R, James GA, Gutman DA, Kilts CD (2015), Organization of intrinsic functional brain connectivity predicts decisions to reciprocate social behavior. Behav Brain Res 292:478-483. doi:10.1016/j.bbr.2015.07.008

Cao H, Plichta MM, Schäfer A, Haddad L, Grimm O, Schneider M, Esslinger C, Kirsch P, et al. (2014), Test–retest reliability of fmri-based graph theoretical properties during working memory, emotion processing, and resting state. NeuroImage 84:888-900. doi:10.1016/j.neuroimage.2013.09.013

Cervenka S, Gustavsson JP, Halldin C, Farde L (2010), Association between striatal and extrastriatal dopamine d2-receptor binding and social desirability. NeuroImage 50:323-328. doi:10.1016/j.neuroimage.2009.12.006

Christ SE, Van Essen DC, Watson JM, Brubaker LE, McDermott KB (2009), The contributions of

prefrontal cortex and executive control to deception: Evidence from activation likelihood estimate meta-analyses. Cereb Cortex 19:1557-1566. doi:10.1093/cercor/bhn189

Cui F, Wu S, Wu H, Wang C, Jiao C, Luo Y (2018), Altruistic and self-serving goals modulate behavioral and neural responses in deception. Soc Cogn Affect Neurosci 13:63-71. doi:10.1093/scan/nsx138

Cui Z, Gong G (2018), The effect of machine learning regression algorithms and sample size on individualized behavioral prediction with functional connectivity features. NeuroImage 178:622-637. doi:10.1016/j.neuroimage.2018.06.001

Cui Z, Su M, Li L, Shu H, Gong G (2018), Individualized prediction of reading comprehension ability using gray matter volume. Cereb Cortex 28:1656–1672. doi:10.1093/cercor/bhx061

Cui Z, Xia Z, Su M, Shu H, Gong G (2016), Disrupted white matter connectivity underlying developmental dyslexia: A machine learning approach. Hum Brain Mapp 37:1443-1458. doi:doi:10.1002/hbm.23112

DePaulo BM, Lindsay JJ, Malone BE, Muhlenbruck L, Charlton K, Cooper H (2003), Cues to deception. Psychol Bull 129:74. doi:10.1037/0033-2909.129.1.74

Dogan A, Morishima Y, Heise F, Tanner C, Gibson R, Wagner AF, Tobler PN (2016), Prefrontal connections express individual differences in intrinsic resistance to trading off honesty values against economic benefits. Sci Rep 6. doi:10.1038/srep33263

Ecker C, Marquand A, Mourão-Miranda J, Johnston P, Daly EM, Brammer MJ, Maltezos S, Murphy CM, et al. (2010), Describing the brain in autism in five dimensions—magnetic resonance imaging-assisted diagnosis of autism spectrum disorder using a multiparameter classification approach. J Neurosci 30:10612-10623. doi:10.1523/jneurosci.5413-09.2010

Egerton A, Rees E, Bose SK, Lappin JM, Stokes PRA, Turkheimer FE, Reeves SJ (2010), Truth, lies or self-deception? Striatal d2/3 receptor availability predicts individual differences in social conformity. NeuroImage 53:777-781. doi:10.1016/j.neuroimage.2010.06.031

Feng C, Zhu Z, Gu R, Wu X, Luo Y-J, Krueger F (2018), Resting-state functional connectivity underlying costly punishment: A machine-learning approach. Neuroscience 385:25-37. doi:10.1016/j.neuroscience.2018.05.052

Finn ES, Shen X, Scheinost D, Rosenberg MD, Huang J, Chun MM, Papademetris X, Constable RT (2015), Functional connectome fingerprinting: Identifying individuals using patterns of brain connectivity. Nat Neurosci 18:1664. doi:10.1038/nn.4135

Fox MD, Snyder AZ, Vincent JL, Corbetta M, Van Essen DC, Raichle ME (2005), The human brain is intrinsically organized into dynamic, anticorrelated functional networks. Proc Natl Acad Sci U S A 102:9673-9678. doi:10.1073/pnas.0504136102

Freeman LC (1978), Centrality in social networks conceptual clarification. Soc Networks 1:215-239. doi:10.1016/0378-8733(78)90021-7

Friston KJ, Williams S, Howard R, Frackowiak RSJ, Turner R (1996), Movement-related effects in fmri time-series. Magn Reson Med 35:346-355. doi:doi:10.1002/mrm.1910350312

Güth W, Schmittberger R, Schwarze B (1982), An experimental analysis of ultimatum bargaining. J Econ Behav Organ 3:367-388. doi:10.1016/0167-2681(82)90011-7

Gabrieli John DE, Ghosh Satrajit S, Whitfield-Gabrieli S (2015), Prediction as a humanitarian and pragmatic contribution from human cognitive neuroscience. Neuron 85:11-26. doi:10.1016/j.neuron.2014.10.047

Gibson R, Tanner C, Wagner AF (2013), Preferences for truthfulness: Heterogeneity among and within individuals. Am Econ Rev 103:532-548. doi:10.1257/aer.103.1.532

Gong Q, Li L, Du M, Pettersson-Yeo W, Crossley N, Yang X, Li J, Huang X, et al. (2013), Quantitative prediction of individual psychopathology in trauma survivors using resting-state fmri. Neuropsychopharmacology 39:681. doi:10.1038/npp.2013.251

Greene JD, Paxton JM (2009), Patterns of neural activity associated with honest and dishonest moral decisions. Proc Natl Acad Sci U S A 106:12506-12511. doi:10.1073/pnas.0900152106

Hahn T, Notebaert K, Anderl C, Teckentrup V, Kaßecker A, Windmann S (2014), How to trust a perfect stranger: Predicting initial trust behavior from resting-state brain-electrical connectivity. Soc Cogn Affect Neurosci 10:809-813. doi:10.1093/scan/nsu122

He Y, Evans A (2010), Graph theoretical modeling of brain connectivity. Curr Opin Neurol 23:341-350. doi:10.1097/WCO.0b013e32833aa567

Huang CL, Yang YK, Chu CL, Lee IH, Yeh TL, Chen PS, Chiu NT (2006), The association between the lie scale of the maudsley personality inventory and striatal dopamine d2/d3 receptor availability of healthy chinese community subjects. Eur Psychiatry 21:62-65. doi:10.1016/j.eurpsy.2005.05.004

Jenkins AC, Zhu L, Hsu M (2016), Cognitive neuroscience of honesty and deception: A signaling framework. Curr Opin Behav Sci 11:130-137. doi:10.1016/j.cobeha.2016.09.005

Kozel FA, Johnson KA, Mu Q, Grenesko EL, Laken SJ, George MS (2005), Detecting deception using functional magnetic resonance imaging. Biol Psychiatry 58:605-613. doi:10.1016/j.biopsych.2005.07.040

Langleben DD (2008), Detection of deception with fmri: Are we there yet? Legal and Criminological Psychology 13:1-9. doi:10.1348/135532507X251641

Li N, Ma N, Liu Y, He X-S, Sun D-L, Fu X-M, Zhang X, Han S, et al. (2013), Resting-state functional connectivity predicts impulsivity in economic decision-making. J Neurosci 33:4886-4895. doi:10.1523/jneurosci.1342-12.2013

Lin Q, Dai Z, Xia M, Han Z, Huang R, Gong G, Liu C, Bi Y, et al. (2015), A connectivity-based test-retest dataset of multi-modal magnetic resonance imaging in young healthy adults. Scientific Data 2:150056. doi:10.1038/sdata.2015.56

Lisofsky N, Kazzer P, Heekeren HR, Prehn K (2014), Investigating socio-cognitive processes in deception: A quantitative meta-analysis of neuroimaging studies. Neuropsychologia 61:113-122. doi:10.1016/j.neuropsychologia.2014.06.001

Liu J, Xia M, Dai Z, Wang X, Liao X, Bi Y, He Y (2017), Intrinsic brain hub connectivity underlies individual differences in spatial working memory. Cereb Cortex 27:5496-5508. doi:10.1093/cercor/bhw317

Luo Y, Kong F, Qi S, You X, Huang X (2015), Resting-state functional connectivity of the default mode network associated with happiness. Soc Cogn Affect Neurosci 11:516.

Maréchal MA, Cohn A, Ugazio G, Ruff CC (2017), Increasing honesty in humans with noninvasive brain stimulation. Proc Natl Acad Sci U S A 114:4360-4364. doi:10.1073/pnas

Meyer ML, Davachi L, Ochsner KN, Lieberman MD (2018), Evidence that default network connectivity during rest consolidates social information. Cereb Cortex:bhy071-bhy071. doi:10.1093/cercor/bhy071

Molenberghs P, Johnson H, Henry JD, Mattingley JB (2016), Understanding the minds of others: A neuroimaging meta-analysis. Neurosci Biobehav Rev 65:276-291. doi:10.1016/j.neubiorev.2016.03.020

Mourão-Miranda J, Bokde ALW, Born C, Hampel H, Stetter M (2005), Classifying brain states and determining the discriminating activation patterns: Support vector machine on functional mri data.

NeuroImage 28:980-995. doi:10.1016/j.neuroimage.2005.06.070
Nash K, Gianotti LRR, Knoch D (2015), A neural trait approach to exploring individual differences in social preferences. Front Behav Neurosci 8. doi:10.3389/fnbeh.2014.00458
Newman ML, Pennebaker JW, Berry DS, Richards JM (2003), Lying words: Predicting deception from linguistic styles. Pers Soc Psychol Bull 29:665-675. doi:10.1177/0146167203029005010
Ofen N, Whitfield-Gabrieli S, Chai XJ, Schwarzlose RF, Gabrieli JDE (2017), Neural correlates of deception: Lying about past events and personal beliefs. Soc Cogn Affect Neurosci 12:116-127. doi:10.1093/scan/nsw151
Power Jonathan D, Cohen Alexander L, Nelson Steven M, Wig Gagan S, Barnes Kelly A, Church Jessica A, Vogel Alecia C, Laumann Timothy O, et al. (2011), Functional network organization of the human brain. Neuron 72:665-678. doi:10.1016/j.neuron.2011.09.006
Reeves SJ, Mehta MA, Montgomery AJ, Amiras D, Egerton A, Howard RJ, Grasby PM (2007), Striatal dopamine (d2) receptor availability predicts socially desirable responding. NeuroImage 34:1782-1789. doi:10.1016/j.neuroimage.2006.10.042
Riggio RE, Friedman HS (1983), Individual differences and cues to deception. J Pers Soc Psychol 45:899-915. doi:10.1037/0022-3514.45.4.899
Schrouff J, Rosa MJ, Rondina JM, Marquand AF, Chu C, Ashburner J, Phillips C, Richiardi J, et al. (2013), Pronto: Pattern recognition for neuroimaging toolbox. Neuroinformatics 11:319-337. doi:10.1007/s12021-013-9178-1
Shen X, Finn ES, Scheinost D, Rosenberg MD, Chun MM, Papademetris X, Constable RT (2017), Using connectome-based predictive modeling to predict individual behavior from brain connectivity. Nat Protoc 12:506. doi:0.1038/nprot.2016.178
Spence SA, Hunter MD, Farrow TF, Green RD, Leung DH, Hughes CJ, Ganesan V (2004), A cognitive neurobiological account of deception: Evidence from functional neuroimaging. Philos Trans R Soc Lond B Biol Sci 359:1755. doi:10.1098/rstb.2004.1555
Sun D, Chan CCH, Hu Y, Wang Z, Lee TMC (2015), Neural correlates of outcome processing post dishonest choice: An fmri and erp study. Neuropsychologia 68:148-157. doi:10.1016/j.neuropsychologia.2015.01.013
Tang H, Mai X, Wang S, Zhu C, Krueger F, Liu C (2016), Interpersonal brain synchronization in the right temporo-parietal junction during face-to-face economic exchange. Soc Cogn Affect Neurosci 11:23-32. doi:10.1093/scan/nsv092
Tang H, Ye P, Wang S, Zhu R, Su S, Tong L, Liu C (2017), Stimulating the right temporoparietal junction with tdcs decreases deception in moral hypocrisy and unfairness. Front Psychol 8. doi:10.3389/fpsyg.2017.02033
Tipping ME (2001), Sparse bayesian learning and the relevance vector machine. J Mach Learn Res 1:211-244.
Wang J, Wang X, Xia M, Liao X, Evans A, He Y (2015), Gretna: A graph theoretical network analysis toolbox for imaging connectomics. Frontiers in Human Neuroscience 9. doi:10.3389/fnhum.2015.00386
Wang J, Zuo X, He Y (2010), Graph-based network analysis of resting-state functional mri. Front Syst Neurosci 4. doi:10.3389/fnsys.2010.00016
Xia M, Wang J, He Y (2013), Brainnet viewer: A network visualization tool for human brain connectomics. PLoS One 8:e68910. doi:10.1371/journal.pone.0068910
Xie S, Yang J, Zhang Z, Zhao C, Bi Y, Zhao Q, Pan H, Gong G (2017), The effects of the x chromosome

on intrinsic functional connectivity in the human brain: Evidence from turner syndrome patients. Cereb Cortex 27:474-484. doi:10.1093/cercor/bhv240
Yan C-G, Wang X-D, Zuo X-N, Zang Y-F (2016), Dpabi: Data processing & analysis for (resting-state) brain imaging. Neuroinformatics 14:339-351. doi:10.1007/s12021-016-9299-4
Yang Y, Raine A, Narr KL, Lencz T, LaCasse L, Colletti P, Toga AW (2007), Localisation of increased prefrontal white matter in pathological liars. Br J Psychiatry 190:174-175. doi:10.1192/bjp.bp.106.025056
Zhang H, Mo L (2016), Mentalizing and information propagation through social network: Evidence from a resting-state-fmri study. Front Psychol 7:1716. doi:10.3389/fpsyg.2016.01716
Zhu L, Jenkins AC, Set E, Scabini D, Knight RT, Chiu PH, King-Casas B, Hsu M (2014), Damage to dorsolateral prefrontal cortex affects tradeoffs between honesty and self-interest. Nat Neurosci 17:1319-1321. doi:doi:10.1038/nn.3798
Zuo X-N, Di Martino A, Kelly C, Shehzad ZE, Gee DG, Klein DF, Castellanos FX, Biswal BB, et al. (2010), The oscillating brain: Complex and reliable. NeuroImage 49:1432-1445. doi:10.1016/j.neuroimage.2009.09.037
Zuo X-N, Xing X-X (2014), Test-retest reliabilities of resting-state fmri measurements in human brain functional connectomics: A systems neuroscience perspective. Neurosci Biobehav Rev 45:100-118. doi:10.1016/j.neubiorev.2014.05.009

Figure Legends

Figure 1. A) Task procedure. All participants played as proposers (P) who could choose to tell the responder (R) the true total of allocation or not in the modified ultimatum game. B) Distribution of participants' actual deception degree in the task.

Figure 2. The prediction schematic flow using the nodal features extracted from resting-state brain network with graph theoretical analysis. Panels A-D showed the steps of data analysis.

Figure 3. Results of prediction of deception degree for each participant using relevance vector regression (RVR) algorithm and leave-one-out cross-validation (LOOCV). Panels A-C shows the correlation between actual and predicted deception

degree derived from Nodal degree centrality (ND) features (A), Nodal efficiency (NE) features (B) and Nodal betweenness centrality (NB) features (C) respectively. Panels D-E presents the permutation distribution of ND (D) and NE (E) features' mean absolute error (MAE). The black solid lines indicated the true MAE in the prediction.

Figure 4. Contributive nodal features in prediction of individualized deception degree (visualized by BrainNet Viewer (Xia et al., 2013)). A) Primarily contributive Nodal degree centrality (ND) features in RVR prediction. B) Primarily contributive Nodal efficiency (NE) features in RVR prediction.

Figure 5. Permutation distribution of prediction using 10-fold CV. A). Permutation distribution of ND features' mean absolute error (MAE). B) Permutation distribution of NE features' mean absolute error (MAE). The black solid lines indicated the mean MAE in the prediction using 10-fold CV.

Table 1. MNI coordinates and weights of primarily contributive nodal degree centrality (ND) features in RVR prediction. L, lfet, R; right.

ROI	Hemisphere	MNI coordinate X	Y	Z	Metric	Weight
Temporal						
Inferior temporal gyrus	L	-50	-7	-39	ND	0.201
	R	46	-47	-17	ND	0.126
	L	-68	-41	-5	ND	0.126
Middle temporal gyrus	L	-56	-13	-10	ND	0.109
	R	65	-31	-9	ND	0.085
Fusiform	L	-31	-10	-36	ND	0.088
Subcortical						
Putamen	L	-31	-11	0	ND	0.171
Thalamus	L	-10	-18	7	ND	0.111
Frontal						
Precentral gyrus	L	-38	-15	69	ND	0.159
	R	38	-17	45	ND	0.102
	L	-32	-1	54	ND	0.092
	R	8	48	-15	ND	0.131
Orbitofrontal cortex	R	8	41	-24	ND	0.113
	R	6	67	-4	ND	0.105
	R	34	38	-12	ND	0.098
Superior frontal gyrus	R	13	-1	70	ND	0.122
	L	-16	-5	71	ND	0.103
	R	10	-17	74	ND	0.090
Middle frontal gyrus	R	47	10	33	ND	0.101
	R	43	49	-2	ND	0.094
Medial frontal gyrus	L	-8	48	23	ND	0.100
Dorsolateral prefrontal cortex	R	13	55	38	ND	0.097
	L	-42	38	21	ND	0.089
Parietal						
Precuneus	L	-7	-52	61	ND	0.112
	L	-16	-77	34	ND	0.089
Postcentral gyrus	L	-54	-23	43	ND	0.107
Temporoparietal junction	R	47	-50	29	ND	0.095
Angular	L	-39	-75	44	ND	0.090
Inferior parietal lobule	R	33	-53	44	ND	0.084
Paracentral lobule	L	-7	-33	72	ND	0.081
Occipital						
Middle occipital gyrus	R	42	-66	-8	ND	0.093
Cerebellum						
Cerebelum	R	35	-67	-34	ND	0.090
	L	-32	-55	-25	ND	0.086

Table 2. MNI coordinates and weights of primarily contributive nodal efficiency (NE) features in RVR prediction. L, lfet, R; right.

ROI	Hemisphere	MNI coordinate X	Y	Z	Metric	Weight
Temporal						
Inferior temporal gyrus	L	-50	-7	-39	NE	0.213
	R	46	-47	-17	NE	0.135
Middle temporal gyrus	L	-68	-41	-5	NE	0.108
Fusiform	R	33	-12	-34	NE	0.125
Subcortical						
Putamen	L	-31	-11	0	NE	0.149
Thalamus	L	-2	-13	12	NE	0.129
	R	12	-17	8	NE	0.103
Frontal						
Medial orbitofrontal cortex	R	6	67	-4	NE	0.142
Superior frontal gyrus	L	-16	-5	71	NE	0.108
	R	10	-17	74	NE	0.105
	R	13	-1	70	NE	0.102
Precentral gyrus	L	-38	-15	69	NE	0.102
Medial frontal gyrus	L	-3	26	44	NE	0.094
	R	43	49	-2	NE	0.094
Dorsolateral prefrontal cortex	L	-42	38	21	NE	0.099
	R	31	33	26	NE	0.087
Parietal						
Superior parietal lobule	L	-16	-46	73	NE	0.131
	L	-28	-58	48	NE	0.104
Inferior parietal lobule	R	33	-53	44	NE	0.107
Temporoparietal junction	R	47	-50	29	NE	0.086
Precuneus	L	-16	-77	34	NE	0.088
Occipital						
Lingual gyrus	R	17	-91	-14	NE	0.111
Middle occipital gyrus	L	-47	-76	-10	NE	0.098
	R	42	-66	-8	NE	0.086
Cerebellum						
Cerebelum	L	-32	-55	-25	NE	0.106

Figure 1

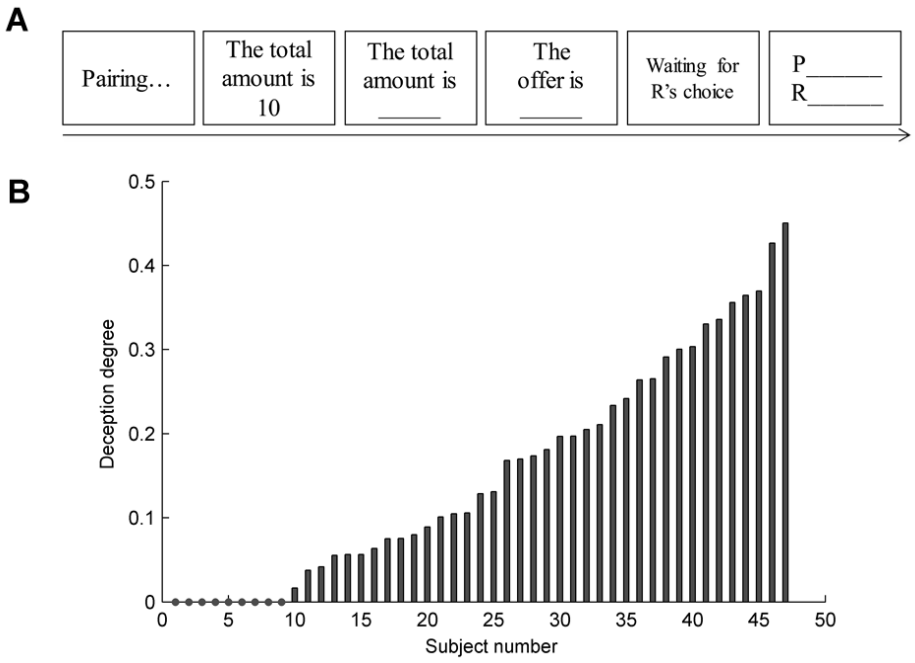

Figure 2

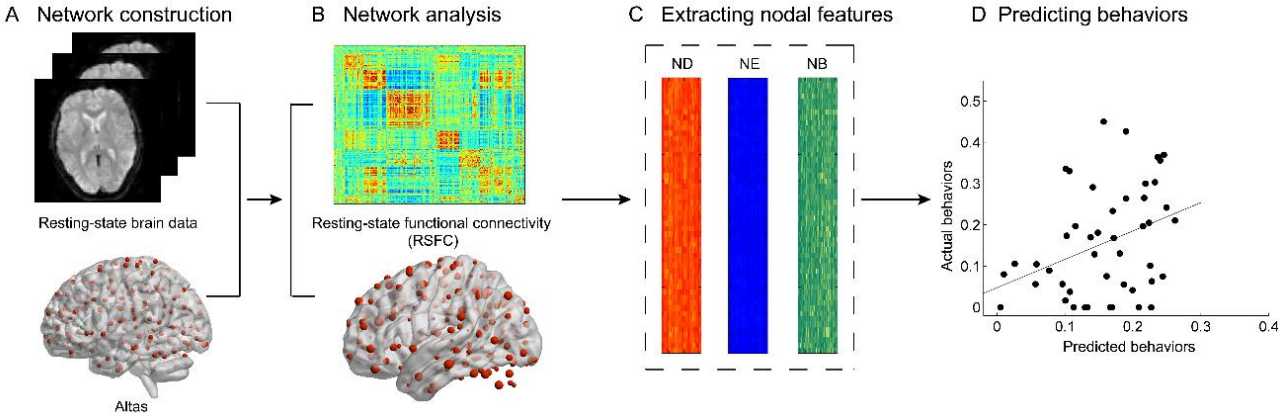

Figure 3

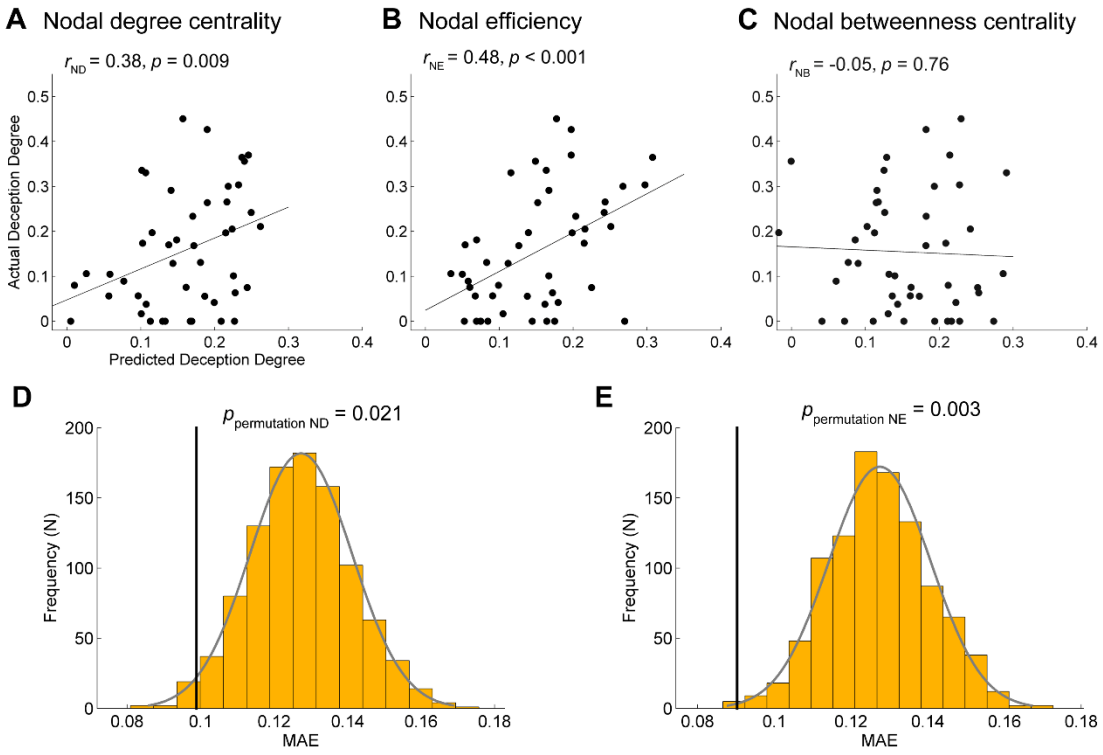

Figure 4

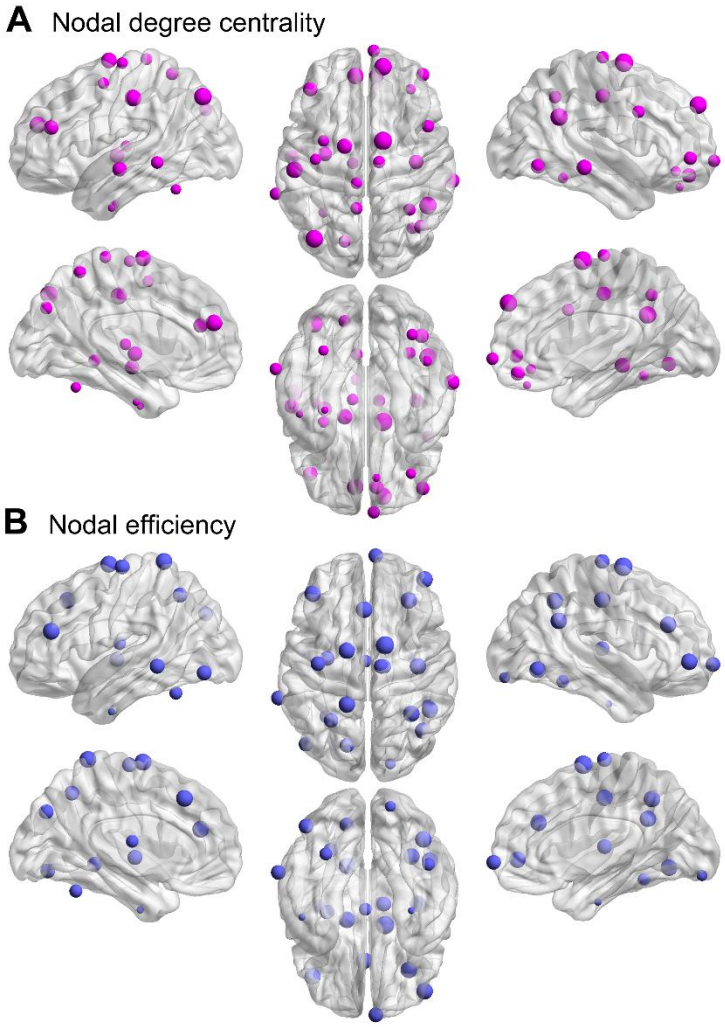

Figure 5

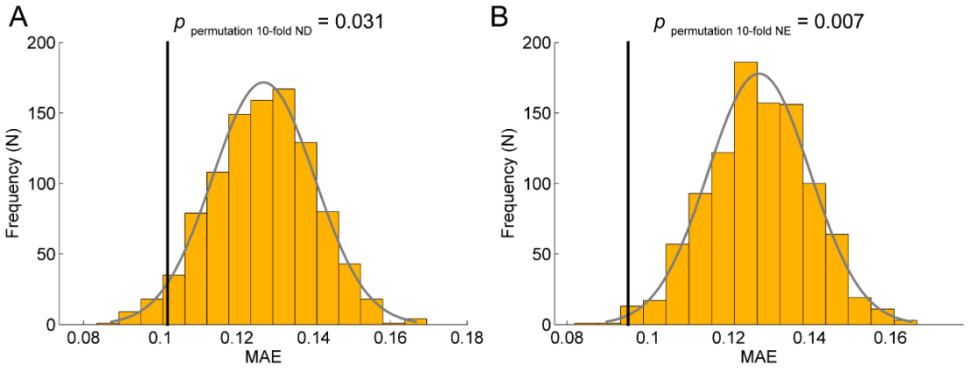

Graphical abstract

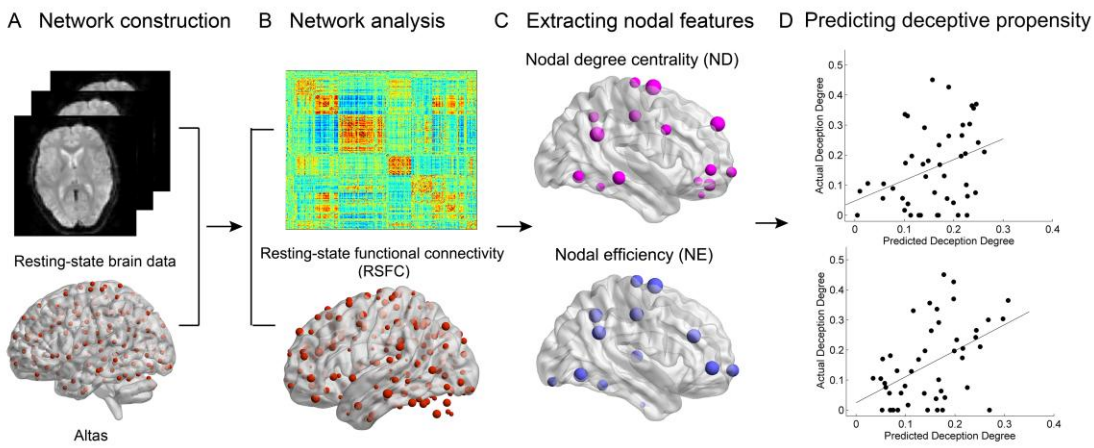

Highlights

1. The neural substrates of individualized deceptive propensity could be captured by resting-state functional connectivity.

2. A relevance vector regression machine-learning approach was used to predict individualized deceptive propensity based on RSFC.

3. Individualized deception was predicted by the executive controlling, the social and mentalizing, and the reward network.

4. These networks have been found to form a signaling cognitive framework of deception in task-dependent fMRI studies.